sustainability

MDPI

Article

Assessing and Predicting Geogrid Reduction Factors after Damage Induced by Dropping Recycled Aggregates

Mateus P. Fleury [1,2,*,†], Gustavo K. Kamakura [1], Cira S. Pitombo [3], André Luiz B. N. Cunha [3], Fernanda B. Ferreira [4] and Jefferson Lins da Silva [1,3]

1 Department of Geotechnical Engineering (SGS), São Carlos School of Engineering (EESC), University of São Paulo (USP), São Carlos 13566-590, SP, Brazil
2 Mauá Institute of Technology (IMT), São Caetano do Sul 09580-900, SP, Brazil
3 Department of Transportation Engineering (STT), São Carlos School of Engineering (EESC), University of São Paulo (USP), São Carlos 13566-590, SP, Brazil; alcunha@usp.br (A.L.B.N.C.)
4 CONSTRUCT, Faculty of Engineering, University of Porto, R. Dr. Roberto Frias, 4200-465 Porto, Portugal
* Correspondence: mateusfleury@usp.br
† Current address: Laboratório de Geossintéticos, Departamento de Geotecnia, Avenida Trabalhador São Carlense, n° 400, São Carlos 13566-590, SP, Brazil.

Abstract: To fulfill the modern concept of sustainable construction, the civil engineering community has shown increased interest in alternative options to replace natural backfills for engineering purposes. Since Recycled Construction and Demolition Waste (RCDW) has proven to be attractive in environmental, economic, and technical aspects, its behavior should be assessed considering its interaction with other construction materials, such as geosynthetics. Bearing in mind that the backfill affects the durability of geosynthetic materials, this study aims to assess the damage caused to geogrids by RCDW dropped by transportation (dump) trucks. Moreover, this study aimed to obtain an equation to predict the reduction factor caused by the backfill drop process. In an experimental facility, six RCDW materials (with different grain size distributions) were dropped (using a backhoe loader) from 1.0 m and 2.0 m heights over three distinct geogrids; the geogrid samples were exhumed and then tested under tensile loading. The results provided a database subjected to machine learning (Artificial Neural Network—ANN) to predict the reduction factor caused by the induced damage. The results demonstrate that the increase in drop height or potential energy cannot be directly associated with the damage. However, the damage increases as the maximum grain size of uniform gradation backfill increases, which is different from the results obtained from the fall of continuous gradation backfill. Moreover, since ANNs do not have any of the traditional constraints that multiple linear regression has, this method is an attractive solution to predict the geosynthetic reduction factors, providing relative errors lower than 8% compared to the experimental investigation reported in the study.

Keywords: sustainable development; recycled aggregates; geosynthetics; artificial neural networks; durability; grain-size distribution

Citation: Fleury, M.P.; Kamakura, G.K.; Pitombo, C.S.; Cunha, A.L.B.N.; Ferreira, F.B.; Lins da Silva, J. Assessing and Predicting Geogrid Reduction Factors after Damage Induced by Dropping Recycled Aggregates. *Sustainability* **2023**, *15*, 9942. https://doi.org/10.3390/su15139942

Academic Editor: Antonio Caggiano

Received: 17 May 2023
Revised: 16 June 2023
Accepted: 20 June 2023
Published: 22 June 2023

1. Introduction

The construction industry uses several types of aggregates in different works, such as concrete production, dams, embankments, and subgrades for railways or highways. Unfortunately, this massive usage requires significant exploitation of natural resources, and the effects of such overexploitation on our world and human health have been addressed by different countries [1–5]. Moreover, the construction industry is also responsible for generating a great deal of construction and demolition waste (CDW). The generators' negligence in the management and correct disposal of CDW, added to the lack of public policies to control this process, has led to other environmental impacts [6–10].

In this context, the construction industry addresses two needs (a decrease in natural resource exploitation and correct management of the CDW generated), which have a common solution: returning residues generated as raw material. However, high physical and chemical heterogeneity harms are caused by directly reusing CDW, which, as it is inappropriately disposed of, may be contaminated by other materials (e.g., non-inert general waste). Nevertheless, adopting a recycling process for CDW provides a material with less heterogeneity (compared to CDW) that has followed standardized procedures. As a result, this strategy (recycling): (i) potentially decreases the demand for natural aggregates; (ii) reduces the environmental impacts related to quarry exploration; (iii) minimizes efforts within CDW disposal; and (iv) provides new raw materials for the construction industry [6–8,11–15].

In a simplified manner, the recycling process involves several steps: receiving, identifying, depositing (stockpiling) CDW, source separation, crushing (hammer or jaw equipment), and removing light contaminants (plastic, cork, rubber, wood, foam, etc.) and iron scraps. Then, the recycled material is sorted by high-frequency vibrating screens into different gradations [16]. The processed material is called 'recycled construction and demolition waste' (RCDW) and comprises different materials. The Brazilian Standard (NBR 15116 [17]) categorizes RCDW into recycled concrete aggregate (RCA) and mixed recycled aggregate (MRA) according to its composition. Other countries consider two additional categories: recycled masonry aggregates (RMA) and recycled asphalt pavement (RAP) [18,19].

To consolidate RCDW as a viable and advantageous alternative for natural aggregates in the market, it must be perceived as such. Designers must also consider essential parameters for a safe and economical design, strengthening its position as a desirable alternative [13]. In the past decades, in addition to the research evaluating the environmental and economic aspects related to using RCDW materials [20–25], several studies have reported the potential substitution of natural aggregates by RCDW materials in pavement layers [6,26–33] and backfill material for geosynthetic reinforced structures [8,12,34–42]. However, Delongui et al. [26] emphasized that the RCDW characteristics are valid for the research's specific application conditions (e.g., type of CDW generated, recycling process). Thus, not only should the RCDW materials' characteristics be accessed, but it is crucial to assess the effects of their contact/interaction with other materials on site.

Particularly in the case of roads, railways, and reinforced structures, RCDW can be used as backfill material and be combined with reinforcement materials, such as geosynthetics. In these applications, additional care must be taken in terms of the geosynthetics' durability. Their physical, mechanical, and hydraulic properties established in the design must be fulfilled to ensure the structure's behavior, reliability, and safety. Among the factors affecting geosynthetics' durability, installation damage, chemical degradation, and creep behavior are pointed out by Allen and Bathurst [43] and FHWA [44] as the most outstanding factors. Numerically, the reduction factors for installation damage (RF_{ID}) and creep behavior (RF_{CR}) are the most significant strength reduction factors [43]. The immediate reduction in mechanical properties caused by installation damage leads to an immediate reduction in the mechanical properties [45] is considered the main factor affecting the geosynthetics' ultimate tensile strength [46]. Consequently, this study focused on assessing the ultimate tensile strength design parameter to evaluate the impact of installation damage.

The geosynthetics installation process comprises backfill material handling, transportation, dropping, strewing, and compaction [47]. Cazzuffi et al. [48] highlighted that the installation damage depends on different factors related to construction activities (especially the installation procedures and compaction) and the materials used (geosynthetics and backfilling material). In recent years, several studies (e.g., [49–53]) have investigated the installation damage on geogrids caused by natural aggregates. Only a few results are available regarding the investigation of installation damage using recycled aggregates. Santos et al. [54] reported that polyester (PET) geogrids exhibited RF_{ID} values equal to 1.12 after lightweight roller compaction and 1.28 for vibratory hammer compaction. Fleury et al. [47] obtained higher RF_{ID} values with the vibratory hammer compaction (1.11) than with the

vibratory roller compaction (1.06) and associated the difference with the degree of soil compaction. The compaction with the vibratory plate used by Vieira and Pereira [55] and Vieira and Lopes [56] and the static compaction performed by Domiciano et al. [57] did not affect the geogrids' mechanical behavior. However, the former study mainly aimed at investigating the chemical and environmental degradation induced by RCDW on the tensile behavior of geosynthetics. Therefore, a lightweight compaction process was adopted to minimize geosynthetic installation damage.

The abovementioned studies investigated the installation damage due to the compaction of the backfill material on the geosynthetics and neglected its dropping effect. In practice, the backfilling material arrives on-site in a dump truck. The material is dropped (by elevating the dump bed), at least from a height of 1.0 m, over the geosynthetic materials. Moreover, considering dropping particles near the top of the pile inside the dump truck, the impact could be with higher energy. Previous studies by Barbosa and Santos [58] and Fleury et al. [47] investigated the damage caused by the backfill drop material. They reported reduction factors lower than 1.12 and highlighted that the damage did not increase with the drop height. Despite these conclusions, these studies have only investigated a single backfill type. Thus, the damage caused by dropping the backfill material on different geosynthetics requires further investigations to be better understood.

Since the geosynthetic durability assessment started in the late 1980s, new studies must be able to predict reduction factors. The technology industry has provided several computational tools that can help engineers. The basic one is linear regression, which aims to establish a linear relationship between two variables. This can evolve into multiple linear regression (MLR), where a dependent variable has a linear relationship with more than one independent variable. This technique requires some specific criteria (multicollinearity, homoscedasticity analyses, and normality tests) to validate its use. These criteria may not be met for more complex databases, requiring other techniques such as machine learning algorithms based on neuron behavior and synaptic functions, termed 'Artificial Neural Networks (ANNs).' The neurons and their bonds comprise a structure (architecture), and a series of equations and algorithms are dedicated to training it to provide accurate outputs and minimize the losses of the input parameters. Unlike MLR, ANNs do not require any criteria to obtain the relationship between independent and dependent variables. Considering geotechnical engineering, ANNs have been used to predict: (i) leakage rates through linear composites [59], (ii) pile's load settlement curve [60], (iii) soil shear strength [61], (iv) the settlement of geosynthetic-reinforced soil foundations [62], and the reduction factor for geotextiles caused by dropping recycled backfill material [63].

This study focuses on assessing and predicting the damage caused by dropping Recycled Construction and Demolition Waste (RCDW) on geogrids. A comprehensive experimental investigation was conducted where different RCDW materials were dropped over three geogrids; the samples were exhumed and tested under short-term tensile loads. The results created databases that were then subjected to machine learning. The objective was to predict reduction factor values that should be considered to better estimate the reduction factor due to installation damage when this damage mechanism (drop height) is considered crucial in design.

2. Materials and Methods

2.1. Geosynthetics

Geogrids are the most common type of geosynthetics used as reinforcement elements. Furthermore, the mechanical characteristics of geosynthetics made of polyester (PET) filaments explain their wide application in Geosynthetic Reinforced Soil (GRS) structures [64]. This study investigated three geogrids commonly used in Brazilian GRS structures: two manufactured with PET yarns and one with poly(vinyl) alcohol (PVA) yarns. The selection criteria were established to evaluate the impact of two factors on the survivability of geogrids: the ultimate tensile strength (comparison between PET geogrids) and the constituent polymer (comparison between PET and PVA geogrids with a similar

ultimate tensile strength). These criteria were utilized to assess the geogrids' resistance to induced damage. Table 1 summarizes the geogrids' properties as provided by the manufacturer. For this study, the geogrids were cut into meshes with 2.40 m in the transversal direction and 1.00 m in the longitudinal direction.

Table 1. Geogrids' properties—as provided by the manufacturer.

Properties	Unit	PET-A	PET-B	PVA
Tensile strength in the machine direction (MD)	kN/m	35	55	35
Deformation at failure in MD	%	≤10	≤10	≤10
Open area	mm	20 × 20	20 × 20	20 × 30
Manufacturing polymer	-	PET	PET	PVA

2.2. Recycled Construction and Demolition Waste (RCDW)

As shown in Section 1, the RCDW can be classified according to their composition. Since the recycling process in Brazil is still incipient and needs government policies and incentives, recycling plants commonly provide mixed materials. For this study, six different materials were provided by a recycling plant that processes CDW using double crushing (jaw crusher). The RCDW characteristics (Table 2 and Figure 1) were evaluated following the Brazilian Association of Technical Standards (ABNT) [65,66].

Table 2. Characteristics of the RCDW materials investigated in this study.

Material	Classification (ASTM D 2487 [67])	C_C	C_U	D_{max} (mm)	Shape Index
SA	SP	0.80	5.00	6.3	n.a
GA	GP	1.59	2.94	>76.0	1.9
GB	GP	1.17	1.78	25.4	2.0
GC	GP	3.69	7.27	19.0	2.1
GG1	SP	0.35	90.00	76.0	2.0
GG2	GP	0.82	42.35	25.4	2.1

Note: GA, gravel A; GB, gravel B; GC, gravel C; SA, sand; GG1, graded gravel one; GG2, graded gravel two; C_C, coefficient of curvature; C_U, coefficient of uniformity; GP, poorly graded gravel with sand; SP, poorly graded sand; n.a, not applicable.

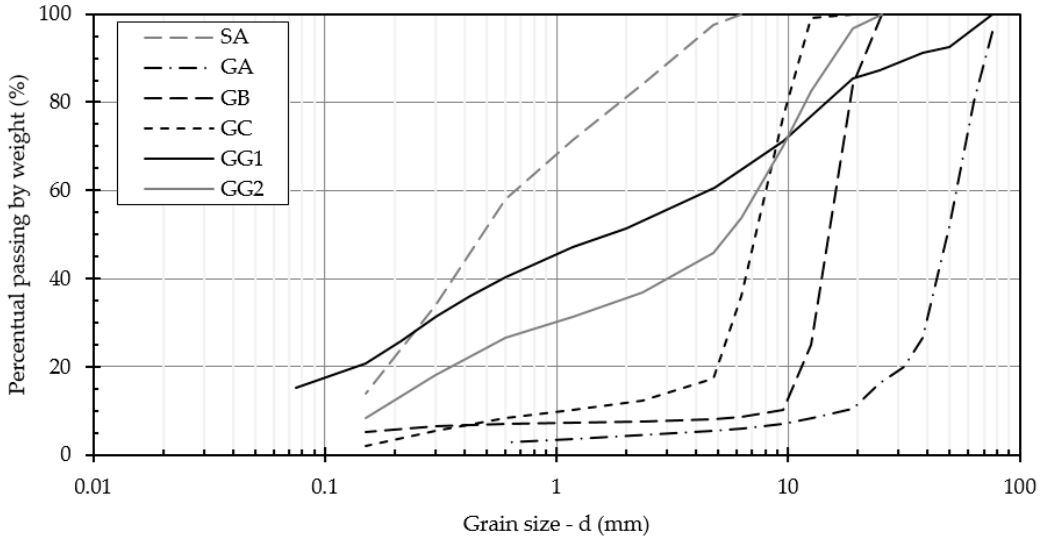

Figure 1. The grain-size distribution curve of the RCDW materials.

2.3. Damage Simulation Procedures

The recycling plant's facility caused the damage caused by dropping backfill materials (RCDW) on geosynthetics (geogrids). The free particles were removed from the surface (manually, using a hoe), and the geogrid meshes were laid over them in the provided area. In the following process, each RCDW material was dropped over a geogrid mesh from 1.0 m (H1) and 2.0 m (H2) heights (each drop height in a different mesh) using the recycling plant's wheel loader. Before dropping the RCDW materials, the wheel loader's operator was always instructed to fill the bucket as much as possible and write down the weight of the RCDW in the bucket. Table 3 shows the average weight, its respective coefficient of variation, and the potential energy (E_p) resulting from the drop of 1.0 m and 2.0 m heights. After dropping all RCDW materials over each mesh, the geogrids were exhumed using a hoe and shovel, avoiding additional damage. The meshes were curled, wrapped in bubble wrap, and transported to the Geosynthetics Laboratory of the São Carlos School of Engineering to perform tensile strength tests. Overall, this process was similar to the ones adopted by Fleury et al. [47], Barbosa and Santos [58], and Barbosa et al. [68]. Figure 2 illustrates some stages of the damage simulation procedure.

Table 3. Potential energy involved in the drop of each backfill from 1.0 m and 2.0 m height.

Material	Bucket Weight (100% Filled)	E_p for 1.0 m	E_p for 2.0 m
SA	3093 kg (3.55%)	30.31 kJ	60.63 kJ
GA	3258 kg (4.82%)	31.93 kJ	63.86 kJ
GB	2140 kg (2.84%)	20.97 kJ	41.94 kJ
GC	2500 kg (3.86%)	24.50 kJ	49.00 kJ
GG1	3473 kg (3.33%)	34.04 kJ	68.08 kJ
GG2	3330 kg (3.60%)	32.63 kJ	65.27 kJ

Note: Coefficient of variation (COV) is presented in parentheses. GA, gravel A; GB, gravel B; GC, gravel C; SA, sand; GG1, graded gravel one; and GG2, graded gravel two.

(**a**) (**b**)

Figure 2. Experimental test to simulate the damage of geosynthetics: (**a**) positioning of the wheel loader for launching the backfill from 2.0 m height; and (**b**) configuration after the dropping process of some scenarios and the start of the geogrids' exhumation.

2.4. Damage Quantification

As recommended by Allen and Bathurst [69], the effects of installation damage on geosynthetic durability must be assessed in terms of (i) ultimate tensile strength (T_{ult}), (ii) strain at failure (ε_f), and (iii) secant tensile stiffness (J_{sec}). These properties of interest were obtained from tensile tests, following ASTM D 6637 [70], performed in seven (7) wide-width specimens (1.00 m long per 0.20 m width) at a 10%/min strain rate using a universal testing machine with a 10 kN load cell. The strains' evolution was measured by a video-extensometer. The tests were performed on undamaged (as received by the manufacturer) and damaged (tests performed after the damage procedures) specimens.

Allen and Bathurst [69] emphasized that monitoring geosynthetic strains is essential to assessing the material's tensile strength evolution. Furthermore, Paula et al. [71] and Huang and Liao [72] considered that geosynthetic tensile stiffness is the best property to characterize the behavior of polymeric materials. Thus, the damage induced in this study was quantified in terms of the reduction factor for each property of interest, which means ultimate tensile strength (RF_T), strain at failure (RF_ε), and secant tensile stiffness at 2% strain (RF_J).

Before calculating the reduction factors, the properties of interest were evaluated regarding their retained value. This value was calculated for each scenario according to Equation (1): the ratio between the property of interest (X) at a given condition (X_c; e.g., damaged) and the mean value of the same property in its undamaged condition ($\overline{X_u}$).

$$RX = {X_c}\Big/{\overline{X_u}} \tag{1}$$

To calculate the reduction factors, a statistical tool was used to establish a confidential interval for each property of interest and validate the damage occurrence. This study assumed a normal population distribution with an unknown standard deviation. These criteria justify adopting the Student's t-distribution. Equation (2) calculates the maximum and minimum values of the confidential interval.

$$X_{max}\ or\ X_{min} = \overline{X_u} \pm {t.s}\Big/{\sqrt{n}} \tag{2}$$

X_{max} and X_{min} represent the confidential interval's maximum and minimum values for the X property; s is the standard deviation, and n is the sample size. The value of the Student's t-distribution variable (t) depends on n and the confidential level (it was set equal to 95% as it is used to calculate the design tensile strength and provide a value similar to the subtraction of two times the standard deviation from the geosynthetics ultimate tensile strength obtained in the laboratory [73]). As the tests were performed on the same number of specimens, this study adopts t equal to 1.9432.

The reduction factors were calculated using two different methodologies. The first one is similar to the traditional method adopted in the literature: the ratio between the mean value of the property of interest in its undamaged condition ($\overline{X_u}$) and the mean value of the same property of interest in its damaged condition ($\overline{X_d}$; Equation (3)). The second method comprises the mean of the ratio between $\overline{X_u}$ and each result (specimen) of the property of interest obtained in the tensile test on damaged conditions (X_{d_s}; Equation (4)). To consider the variability of the undamaged samples, if $\overline{X_d}$ or $\overline{X_{d\_s}}$ were equal to or higher than X_{min}, it indicates doubt related to the damage occurrence (as the damaged value is inside the variability of the undamaged materials). In this case, the reduction factor assigned is equal to 1.00 (Equation (5)).

$$FR_X = {\overline{X_u}}\Big/{\overline{X_d}} \rightarrow if\ \overline{X_d} < X_{min} \tag{3}$$

$$FR_X = \overline{{\overline{X_u}}\Big/{X_{d\_s}}} \rightarrow if\ \overline{X_{d\_s}} < X_{min} \tag{4}$$

$$FR_X = 1 \rightarrow if \begin{cases} \overline{X_d} \geq X_{min} \\ \quad or \\ \overline{X_{d\_s}} \geq X_{min} \end{cases} \tag{5}$$

2.5. Prediction of Reduction Factor Related to the Ultimate Tensile Strength

Two databases were created based on the results obtained in this study to predict the reduction factors. The first one comprises the reduction factor calculated based on the first method adopted (Equations (3) and (5)), with 36 values (one for each scenario investigated).

The second one is based on the second method adopted to calculate the reduction factors. As seven specimens were tested under damaged conditions, the mean undamaged specimens' value was divided by the result of each damaged specimen, providing seven pieces of data (reduction factor values) for each scenario. Thus, this second database comprises a total of 252 values (data). These databases were created merely for the geogrids' ultimate tensile strength.

The backfills' data were entered into the database according to their classification as per ASTM D 2487 [67] to provide a more general equation. The data on the databases were arranged to separate all variables investigated in the study: two drop heights, three geogrids, and two backfill materials (according to their classification in Table 2), and the reduction factor related to the combination of the other variables. Thus, the data were arranged in a dichotomous way, where the presence of a variable in the scenario resulted in a value equal to 1, and, on the contrary, it was set to 0. This process was applied to both databases.

2.5.1. Prediction Using Artificial Neural Networks (ANNs)

Artificial neural networks (ANNs) were used to predict the reduction factors. In this case, an open-source software package (RStudio, PBC; Version 2022.07.2) constructed the ANN algorithms, trained them, and predicted the reduction factor values. Firstly, a sensitivity analysis was made to assess the most viable architecture (one that provides good accuracy with as little computational effort as possible). In R Studio, the data were randomly selected using a routine to split the database into two sets with a desired ratio. As Raschka and Mirjalili [74] suggested, 70% of the data were dedicated to a training set and 30% to the testing set—the procedure applied to both databases. Then, the number of layers in the ANN's architecture varied. With a defined architecture, the sensitivity analyses continued by assessing the most suitable ratio between training and test sets. Using both databases, the ratio that provided the most suitable relative error was adopted to predict the reduction factors. The predicted reduction factor results were compared with the data in both training and testing sets. The accuracy of the reduction factors' prediction was also quantified based on the relative error (Equation (6)). Posteriorly, we compared the predictions made by ANN algorithms, considering the calibration of a traditional technique (Multiple Linear Regression).

$$RE = {|RF_e - RF_p|}\Big/{RF_e} \quad (6)$$

where RE is the relative error; RF_e is the reduction factor obtained by the experimental tests performed in this study; and RF_p is the predicted reduction factor using the model.

2.5.2. Prediction Using Multiple Linear Regression (MLR)

Multiple linear regression (MLR) was applied to both databases using the Stepwise model. The software RStudio (PBC; Version 2022.07.2) was used to apply this method. The use of MLR is justified mainly for methodological validation purposes. We aimed to observe the advantages of using ANNs to predict the reduction factor, as this algorithm has no traditional mathematical constraints. Similar to the ANN's data division, 70% of the data was dedicated to a calibration set and 30% to a validation set—the procedure applied to both databases. The data used for calibration and validation was the same as the one used in the ANN method (in that case, named training and testing sets). Multicollinearity analyses assessed the correlation coefficients between the independent variables (drop height, backfill, and geogrid). Highly correlated variables can make the model sensitive to small changes and reduce the ability to detect significant variables. In the following stage, homoscedasticity analyses and normality tests were performed on the residues obtained by the Stepwise model. Similar to the ANN methodology, the predicted reduction factor results were compared with the training and testing sets' data. The method's accuracy was evaluated based on the relative error (Equation (6)).

3. Results

3.1. Tensile Tests in an Undamaged Condition

Table 4 summarizes the mean and the COV values of the properties of interest obtained after the tensile tests performed on the undamaged specimens, which means the ones tested as received from the manufacturers. The ultimate tensile strength values obtained in the tests were lower than those in the manufacturer's specification. It should be mentioned that the undamaged values of the properties of interest were taken as reference values for the reduction factors' calculation. Additionally, the meshes of each geogrid were obtained from its respective roll. As a result, these results represented the whole roll and did not affect the study.

Table 4. Results of tensile tests performed on undamaged specimens: mean values, coefficient of variation, and confidential interval for each property of interest.

Properties of Interest	PET-A	PET-B	PVA
$\overline{T_{ult}}$ (kN/m)	29.74	44.54	28.34
COV (%)	3.77	6.96	3.91
Confidential interval (kN/m)	30.78–28.70	47.41–41.68	29.37–27.32
$\overline{\varepsilon_f}$ (%)	8.18	7.30	5.02
COV (%)	4.65	8.86	10.27
Confidential interval (%)	8.53–7.82	7.89–6.70	5.54–5.49
$\overline{J_{sec}}$ (kN/m)	400.13	704.34	518.23
COV (%)	6.03	5.32	17.23
Confidential interval (kN/m)	422.44–377.82	739.02–669.67	600.82–435.64

As expected, Table 4 shows a slight variability in the geogrids' ultimate tensile strength (COV values lower than 7.0%). However, significant variability (higher than 10%) was observed in the PVA-based material for the elongation at break and the secant tensile stiffness. Since the t-Student's equation was used to set the undamaged property confidential interval, it became broader as the properties' variability increased. Thus, the reduction factor calculation considered the undamaged properties' variability. Table 4 exhibits the confidential interval for each property of interest.

3.2. Reduction Factors Obtained after the Damage Procedures

3.2.1. Ultimate Tensile Strength

Figure 3 shows the geogrids' retained tensile strength (RTS) after the damage procedures. The vertical bars indicate the mean RTS value, and the error bars show the variability (the maximum and minimum RTS values) among the seven specimens tested. The range between horizontal lines of the same type (continuous or dashed) represents a geogrid's confidential interval. Although the boundary values of the confidential interval of PET-A and PVA are not the same (Table 4), when their values are presented in terms of RTS values (Equation (1)), the confidential interval becomes very close, which is the reason why they look overlapped in Figure 3.

The PET-A geogrid exhibited a significant decrease (RTS value lower than the minimum value of the material's confidential interval for the tensile strength) in its mean undamaged ultimate tensile strength ($\overline{T_u}$) for most scenarios evaluated. The drop of GC from 1.0 m or 2.0 m and GG1 from 1.0 m resulted in a decrease in $\overline{T_u}$, but within the material's confidential interval. Considering the backfill drop with a more uniform grain size distribution, the damage increased as the maximum grain size increased (GC, GB, and GA, in this order; see Figure 1). Thus, the backfill with the highest maximum grain size (GA) is the most aggressive to PET-A geogrid. These results follow other studies [52,53,75–77] that reported a damage increase as the grain size increased. As expected, the backfill drop is more aggressive from 2.0 m (9.68% decrease in $\overline{T_u}$) than when dropped from 1.0 m (7.7% decrease in $\overline{T_u}$) for the GA backfill material. The drop of GB and GG1 follows the same trend: greater damage when dropped from 2.0 m than from 1.0 m. However, the drop of

SA and GG2 backfills contradicts this assumption. In fact, these materials (SA and GG2) caused a similar reduction when they dropped from 1.0 m (7.36%) and 2.0 m (5.43%). These results may indicate that the damage caused by the drop of backfills with continuous grain size distribution is primarily influenced by their curvature (note that SA and GG2 exhibit similar values of C_c; see Table 2). The maximum grain size can be considered a secondary factor in this case, as the reduction in $\overline{T_u}$ value increases with the maximum grain size of the backfills (reductions equal to 5.11%, 5.75%, and 9.67% for SA, GG2, and GG1, respectively, when dropped from 2.0 m).

Although the PET-B geogrid is manufactured from the same polymer as the PET-A geogrid, it has proven to be more resistant to the damage caused by the drop height. Significant reductions in PET-B's $\overline{T_u}$ value occurred when GA was dropped (6.63% reduction for 1.0 m and 8.15% reduction for 2.0 m). Some scenarios have resulted in slight reductions inside the geogrid's confidential interval for $\overline{T_u}$. Comparing the results of PET-made geogrids, PET-B has a more robust structure (to comprise a greater amount of PET fibers) than the PET-A geogrid, which leads to higher resistance to the damage induced. Thus, the damage proves to be more severe when the geogrid structure consists of thinner ribs, as the stress concentration due to the drop tends to be higher. Lim and McCartney [52] also reported the effects of the geogrids' structure on their resistance to damage occurrence. Notwithstanding, Paula et al. [78] also reported that the geogrids' resistance to installation damage increases as the material's ultimate tensile strength increases.

Figure 3 shows that the PVA geogrid was more affected than the PET-made geogrids. While handling the PVA geogrid, it was noted that it presents less cover and lower bending stiffness (not its stiffness under tensile) than the PET geogrids. The lack of cover makes the fibers more susceptible to damage. The high flexibility of the PVA geogrid impairs the energy distribution resulting from the drop of the backfill as it occurs on the PET-made geogrids.

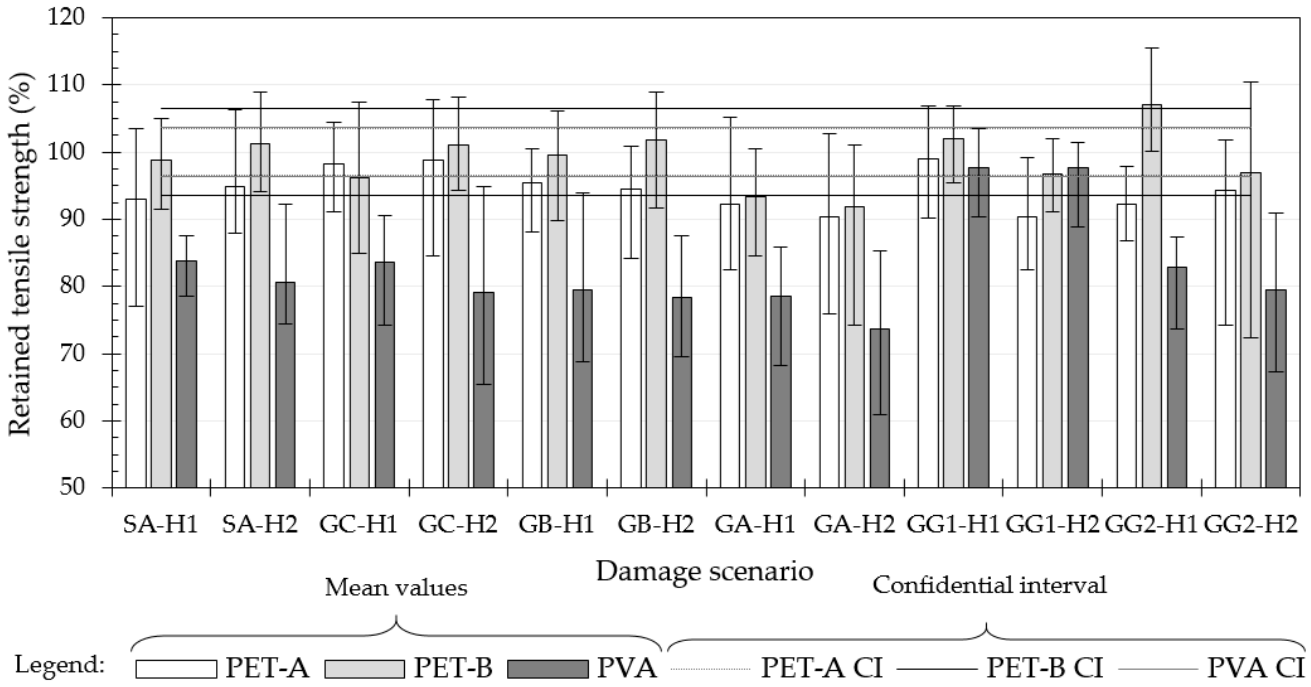

Figure 3. Residual tensile strength was calculated based on each material's undamaged mean tensile strength. [Notes: The vertical bars represent the mean value, the error bars indicate the maximum and minimum values obtained for the seven specimens tested, and the horizontal lines show the confidential intervals' limits of the undamaged tensile strength of each material—PET-A and PVA are overlapped].

PVA geogrid was slightly affected when the GG1 material was dropped, causing a reduction (close to 2.26%) inside the material's confidential interval for $\overline{T_u}$, regardless of the drop height. This milder damage can be associated with two facts: (i) as GG1 exhibits a very continuous distribution (a wide range of grains in its composition), it leads to less damage due to better stress distribution, and (ii) the small open area between the geogrid elements (ribs) promoted a better distribution of the stress compared to the one occurred with the PET geogrids. Considering the other backfill materials, PVA geogrid has suffered reductions ranging between 16.24% (SA drop from 1.0 m; scenario SA-H1) and 26.33% (GA drop from 2.0 m; scenario GA-H2). Similar to the PET-A geogrid, the damage increased with the maximum grain size (GC, GB, and GA, in this order, regardless of the drop height), considering the backfills with a more uniform distribution. For the other backfills with continuous grain-size distribution (SA and GG2), they induced similar reductions in the geogrid's $\overline{T_u}$ value when dropped from 1.0 m (16.67%) and 2.0 m (19.90%). This emphasizes that the damage caused by the drop of continuous backfills is primarily influenced by its curvature, followed by the backfill's maximum grain size.

Although this study investigated backfills with different grain-size distributions, it was not possible to identify a strong relationship between the backfills' grain-size distribution parameters (D_{max}, D_{60}, D_{10}, C_c, or C_u,) and the geogrids' retained tensile strength (RTS). As the results pointed out, the best relationship was between the maximum grain size of the backfills with a more uniform gradation (GA, GB, and GC) and the RTS values (Figure 4a). The coefficients of determination (R^2) for the PET geogrids demonstrate a good relationship (mean R^2 value equal to 0.79), but for the PVA geogrid, the results do not reveal such a satisfactory relationship (R^2 = 0.47). Similarly, an attempt was made to identify a relationship between the potential energy involved in the dropping process and the geogrids' RTS values. However, the data was too vague (Figure 4b), preventing further conclusions.

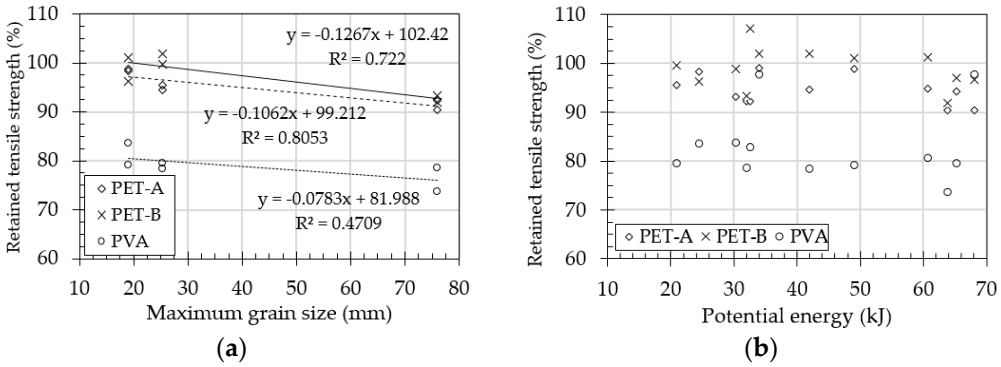

Figure 4. Relationship between the geogrids' retained tensile strength and (**a**) the maximum grain size of the backfill material with a more uniform gradation (GA, GB, and GC), and (**b**) the potential energy involved in the drop process.

Regarding the reduction factors related to the ultimate tensile strength, Table 5 shows the reduction factors calculated by the first method adopted in this study (Equations (3) and (5)). As previously mentioned, the PVA geogrid was the most affected material and exhibited reduction factors ranging between 1.11 and 1.36 (excluding scenarios GG1-H1). PET-B geogrid experienced damage outside its undamaged confidential interval when the GA backfill was dropped, resulting in reduction factors close to 1.08 regardless of the drop height. The PET-A geogrid shows reduction factors equal to or higher than those of the PET-B geogrid. Unlike the results reported by Vieira and Pereira [55], the second method adopted to calculate the reduction factors (Equations (4) and (5)) proves to be a more conservative approach. This method resulted in reduction factor values (Table 6), on average, 2.24% higher than the values calculated using the first method. Overall, the reduction factors related to the backfill drop are lower than those related to the backfill's compaction reported in the literature. For instance,

Huang [75] reported values ranging between 0.95 and 2.01, and Fleury et al. [47] reported a more comprehensive range, 0.83 to 2.33. It is noteworthy that this study does not aim to suggest incorporating an additional reduction factor to calculate the geosynthetic design tensile strength. Rather, the main purpose is to quantify the specific contribution of the drop process of the backfill material over the geosynthetic to the overall geosynthetic damage induced during installation in the field. The results elucidate that the backfill drop causes damage to the geosynthetics. Hence, it must be correctly addressed and considered when it is considered a critical process at the workstation.

Table 5. Reduction factor, calculated by the first method (Equations (3) and (5)), for damage caused by dropping the backfilling material related to the ultimate tensile strength.

RCDW	Drop from 1.0 m			Drop from 2.0 m		
	PET-A	PET-B	PVA	PET-A	PET-B	PVA
SA	1.07	1.00	1.19	1.05	1.00	1.24
GA	1.08	1.07	1.27	1.11	1.09	1.36
GB	1.05	1.00	1.26	1.06	1.00	1.28
GC	1.00	1.00	1.20	1.00	1.00	1.26
GG1	1.11	1.00	1.00	1.00	1.00	1.11
GG2	1.08	1.00	1.21	1.06	1.00	1.26

Table 6. Reduction factor, calculated by the second method (Equations (4) and (5)) for damage caused by dropping the backfilling material, related to the ultimate tensile strength.

RCDW	Drop from 1.0 m			Drop from 2.0 m		
	PET-A	PET-B	PVA	PET-A	PET-B	PVA
SA	1.09	1.03	1.20	1.07	1.01	1.25
GA	1.10	1.07	1.28	1.12	1.10	1.37
GB	1.05	1.03	1.27	1.06	1.02	1.29
GC	1.03	1.06	1.20	1.04	1.01	1.29
GG1	1.03	1.01	1.04	1.11	1.03	1.03
GG2	1.09	1.00	1.21	1.08	1.06	1.27

3.2.2. Strain at Failure

Figure 5 shows the geogrids' retained strain at failure after the damage procedures. The vertical bars indicate retained strain at the failure mean value. The error bars show variability (the maximum and minimum retained strain at failure values) among the seven specimens tested. The range between horizontal lines of the same type (continuous or dashed) represents a geogrid's confidential interval. Two particular scenarios resulted in decreases in the strain at failure below the minimum boundary of the geogrids' confidential interval: PET-A-GG1-H2 (4.22% reduction) and PET-B-GG1-H2 (12.45% reduction). Interestingly, this backfill material resulted in the geogrids' lowest values of retained strain at failure, indicating that it is the most aggressive material regarding this property. A possible explanation is that the better stress distribution resulted from its continuous particle size distribution, which demanded the stretching of the whole mesh. However, this is a specific result that leads to such speculation. The most relevant impact of these results is the wide variability of the strain at failure after the damage is induced. The studies reported by Hsieh and Wu [51] also showed significant variability in the strain at failure after mechanical damage.

Based on the results reported, most reduction factors (calculated following the first method described in Section 2.4) exhibit a value equal to unity (Table 7). Once again, the second method to calculate the reduction factor provides values (Table 8) equal to or higher than those obtained by the first method. The high variability in the retained strain at failure can justify this increase in the reduction factor calculated by the second

method. The reduction factors reported by Hsieh and Wu [51] ranged between 0.88 and 1.41. Thus, although most of the results indicate that the damaged strain at failure has been maintained inside the geogrids' confidential interval for this property, significant variability is associated with the geogrids' strain at failure after the damage is induced.

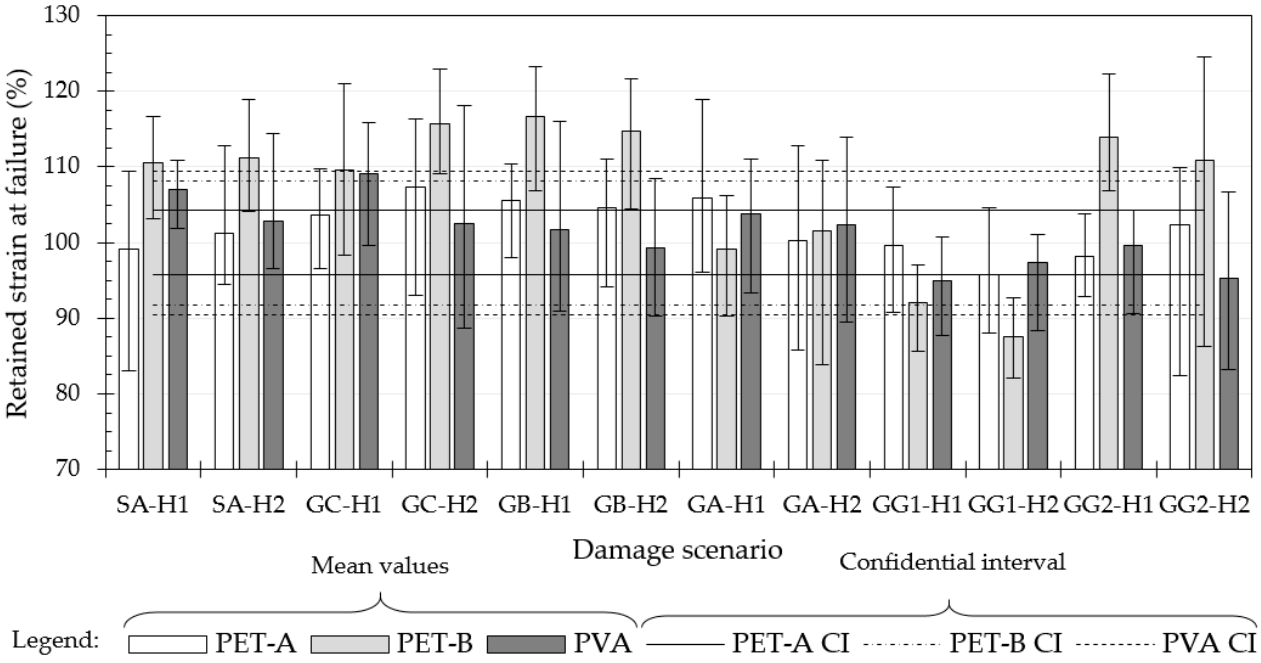

Figure 5. Residual strain at failure is calculated based on each material's undamaged mean strain at failure. [Notes: The vertical bars represent the mean value, the error bars indicate the maximum and minimum values obtained in the seven specimens tested, and the horizontal lines show the confidential intervals' limits of the undamaged strain at failure of each material].

Table 7. The reduction factor for damage caused by dropping the backfilling material is related to the strain at failure calculated by the first method (Equations (3) and (5)).

RCDW	Drop from 1.0 m			Drop from 2.0 m		
	PET-A	PET-B	PVA	PET-A	PET-B	PVA
SA	1.00	1.00	1.00	1.00	1.00	1.00
GA	1.00	1.00	1.00	1.00	1.00	1.00
GB	1.00	1.00	1.00	1.00	1.00	1.00
GC	1.00	1.00	1.00	1.00	1.00	1.00
GG1	1.00	1.00	1.00	1.14	1.04	1.00
GG2	1.00	1.00	1.00	1.00	1.00	1.00

Table 8. The reduction factor for damage caused by dropping the backfilling material is related to the strain at failure calculated by the second method (Equations (4) and (5)).

RCDW	Drop from 1.0 m			Drop from 2.0 m		
	PET-A	PET-B	PVA	PET-A	PET-B	PVA
SA	1.07	1.00	1.04	1.03	1.00	1.03
GA	1.01	1.00	1.03	1.04	1.00	1.06
GB	1.00	1.00	1.04	1.01	1.00	1.02
GC	1.00	1.00	1.00	1.01	1.00	1.08
GG1	1.06	1.06	1.03	1.06	1.11	1.08
GG2	1.03	1.00	1.06	1.01	1.02	1.10

3.2.3. Secant Tensile Stiffness at 2% Strain

Similar to Sections 3.2.1 and 3.2.2, Figure 6 shows the geogrids' retained secant tensile stiffness (RSTS) at 2% strain after the damage procedures. The vertical bars indicate the RSTS mean value, and the error bars show its variability (the maximum and minimum RSTS values) among the seven specimens tested. The range between horizontal lines of the same type (continuous or dashed) represents a geogrid's confidential interval. Figure 6 shows a significant difference between the geogrids' confidential intervals for this property of interest. While the PET geogrids have a similar range, the PVA geogrid shows a much more comprehensive range resulting from the high variability (COV = 17.23%; Table 4) of this parameter for the undamaged (as received) specimens. Another important aspect is the high variability in the results, as reflected by the range between the maximum and minimum data bars. This high variability is not associated solely with the materials' behavior. Fleury et al. [47] pointed out that the method adopted to monitor strain evolution (only in a single longitudinal rib) contributes to increased property variability.

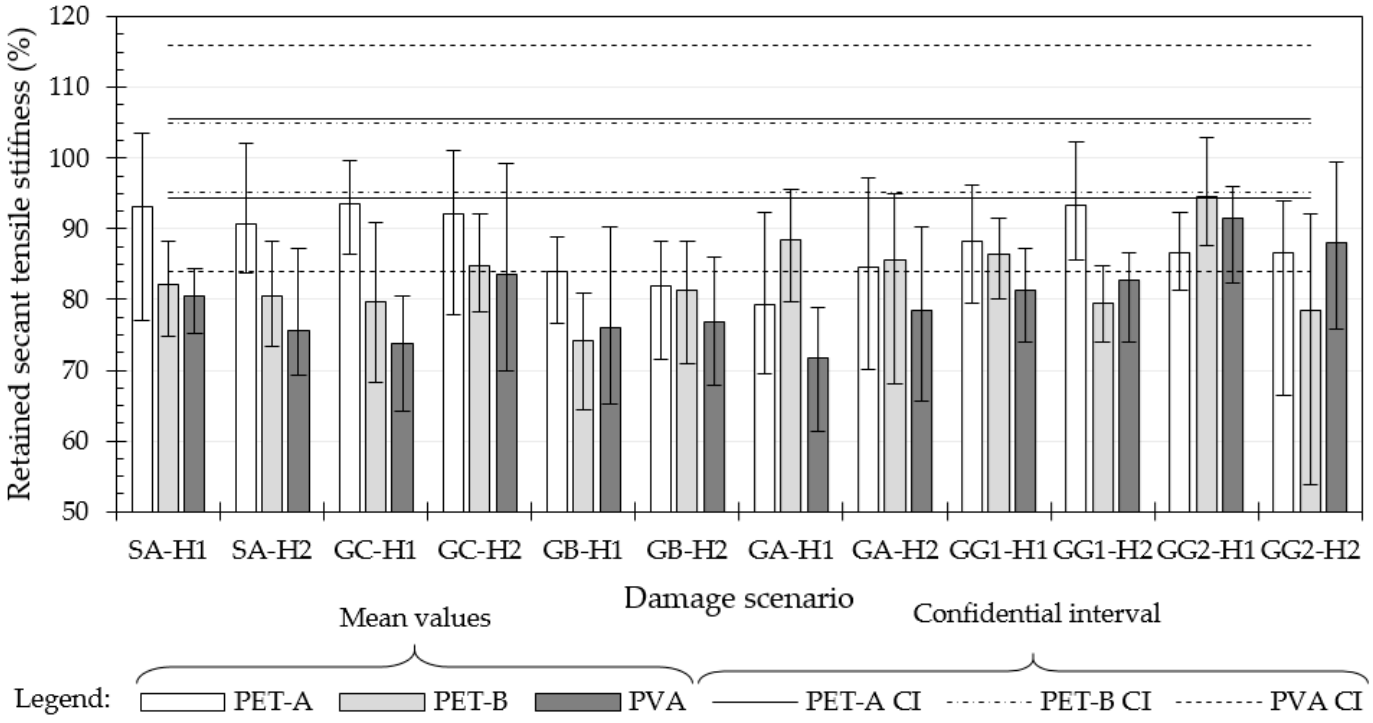

Figure 6. Residual secant tensile stiffness is calculated based on each material's undamaged mean secant tensile stiffness at 2% strain. [Notes: The vertical bars represent the mean value, the error bars indicate the maximum and minimum values obtained in the seven specimens tested, and the horizontal lines show the confidential intervals' limits of the undamaged secant tensile stiffness at 2% strain of each material].

The induced damage significantly affected the secant tensile stiffness of all geogrids investigated. The PET-A geogrid presented mean values of RSTS lower than its confidential interval for all scenarios investigated. Similar to the tensile strength results, the damage caused by the backfill drop with more uniform gradation was higher for the 2.0 m drop height than the 1.0 m drop height (except for the GA material). Moreover, the GA and GB materials were the most aggressive concerning this property, emphasizing that the maximum grain size significantly influences the damage caused by backfills with uniform gradation. Two backfills with continuous gradation led to a similar reduction in the secant tensile stiffness regardless of the drop height: 8.2% for SA and 13.40% for GG2. However, the other material (GG1) shows a considerable

difference between the reduction caused by the drop from 1.0 m (11.61%) and 2.0 m (6.61%). Thus, the first impression obtained by assessing the PET-A geogrid's retained secant tensile stiffness indicates that the damage caused by the different backfill drops affects this property differently.

Contrary to the tensile strength and strain at failure results, the secant tensile stiffness of PET-B geogrid was significantly affected by the backfill drop, especially from the 2.0 m height. Moreover, the secant tensile stiffness of the PET-B geogrid was more affected than that of the PET-A geogrid. The results were more scattered for the more uniform materials (GA, GB, and GC), not indicating a relationship between the damage caused and the maximum particle size. Furthermore, the drop of GC and GB backfills from 1.0 m height caused more considerable damage than that caused by the higher drop height (2.0 m). The opposite behavior can be observed for the materials with continuous gradation: damage caused by the drop height of 2.0 m is greater than that caused by the 1.0 m drop height. Furthermore, there is no correlation between the maximum grain size and the geogrid damage caused by the continuous backfill material.

Similar to the other properties, the PVA geogrid is the most affected by the backfill drop regarding the secant tensile stiffness. Although the GG2 material induced a high decrease in this property, the values were inside the PVA's geogrid confidential interval. When dropped from 1.0 m height, the backfill materials with uniform gradation induced a higher decrease in this property than their drop from 2.0 m, contradicting the results of tensile strength. Considering the continuous backfill materials, the results were even more scattered.

Overall, the geogrids' secant tensile stiffness has proven to be the most affected property with respect to the damage caused by dropping the backfill materials. Although the results did not indicate a standard behavior in the reductions of this property, the impact caused by the drop height has induced elastic deformation on the geogrids that has influenced their stiffness. However, it must be highlighted that this property exhibited significant variability due to the heterogeneity of the damage that occurred and the strain measurement method adopted. Thus, this assumption must be considered cautiously.

Regarding the reduction factor related to the secant tensile stiffness, Table 9 shows values ranging from 1.00 to 1.39, considering the first calculation method adopted in this study. These values are above the ones reported by Pinho-Lopes and Lopes [53] (ranging from 0.99 to 1.07) but lower than the values reported by Hsieh and Wu [51] (0.83 to 1.74). The second method used to calculate the reduction factor resulted in values (Table 10), on average, 2.3% higher than those obtained from the first. This emphasizes that this second method tends to be conservative. It must be highlighted that, for some scenarios, the difference between the values calculated by the first and second methods reaches 10%. In such cases, the second method seems even more conservative.

Table 9. The reduction factor for damage caused by dropping the backfilling material is related to the secant tensile stiffness at 2% strain calculated by the first method (Equations (3) and (5)).

RCDW	Drop from 1.0 m			Drop from 2.0 m		
	PET-A	PET-B	PVA	PET-A	PET-B	PVA
SA	1.07	1.22	1.24	1.10	1.24	1.32
GA	1.26	1.13	1.39	1.18	1.17	1.27
GB	1.19	1.35	1.32	1.22	1.23	1.30
GC	1.07	1.26	1.36	1.09	1.18	1.20
GG1	1.00	1.00	1.23	1.00	1.00	1.21
GG2	1.15	1.06	1.00	1.16	1.27	1.00

Table 10. The reduction factor for damage caused by dropping the backfilling is material related to the secant tensile stiffness at 2% strain calculated by the second method (Equations (4) and (5)).

RCDW	Drop from 1.0 m			Drop from 2.0 m		
	PET-A	PET-B	PVA	PET-A	PET-B	PVA
SA	1.10	1.29	1.27	1.03	1.25	1.33
GA	1.27	1.14	1.40	1.18	1.18	1.36
GB	1.22	1.38	1.32	1.22	1.24	1.27
GC	1.08	1.29	1.36	1.08	1.19	1.30
GG1	1.00	1.00	1.18	1.00	1.00	1.11
GG2	1.16	1.08	1.05	1.17	1.28	1.10

3.3. Prediction of Reduction Factors

3.3.1. Artificial Neural Networks

Tables 11 and 12 show the sensitivity test results performed to identify the best architecture of the ANN and the most suitable ratio between training and testing sets. The increase in nodes in the hidden layers of the ANN (see Figure 7) did not significantly increase the accuracy of the ANN (Table 11). Furthermore, increasing nodes requires more computational effort and would result in a more complex equation (as the number of nodes in the hidden layers increases) to predict the reduction factor values. Table 12 shows that the ratio 60/40 (60% of data for training and 40% for testing) provides one of the lowest relative errors (RE), regardless of the database. Based on the results of this sensitivity analysis (a single hidden layer and a 60/40 ratio), the ANN algorithms were constructed, as illustrated in Figure 7.

Table 11. The relative error in predicting the reduction factors for different Artificial Neural Network architectures based on the numeric database with 36 data.

Training Set (%)	Test Set (%)	Hidden Layers	*RE* (%)
70	30	1	7.37
70	30	2	8.45
70	30	3	7.39
70	30	c(1,1)	7.38
70	30	c(1,2)	7.37
70	30	c(2,1)	7.85
70	30	c(2,2)	5.74
70	30	c(3,1)	6.83

Table 12. The relative error in the prediction of the reduction factors for different ratios between the training and test sets is based on the dichotomous databases.

Training Set (%)	Testing Set (%)	Hidden Layers	36 Data Database	252 Data Database
90	10	1	9.76	7.45
80	20	1	4.64	7.48
70	30	1	5.69	7.52
60	40	1	3.37	7.52
50	50	1	5.09	7.83
40	60	1	4.23	7.94
30	70	1	8.29	8.20
20	80	1	9.58	8.33
10	90	1	9.23	8.59

For the ANN shown in Figure 7, the summation function (u) is given by Equation (7). The activation function (a_f) in Equations (8) and (9) shows the reduction factors' (RF) prediction equation. The weights used in the equation are indicated in Table 13 for both databases.

$$u = w_H + w_{GGR} + w_B + b_1 \tag{7}$$

$$a_f = \frac{1}{1 + \exp(-u)} \tag{8}$$

$$RF = a_f \cdot w_8 + b_2 \tag{9}$$

where w_H, w_{GGR}, and w_B are weights related to the drop height, geogrid type, and backfill material's classification, respectively; b_1 and b_2 are the weights related to the bias involved in the Artificial Neural Networks; and w_8 is the weight that multiplies the activation function.

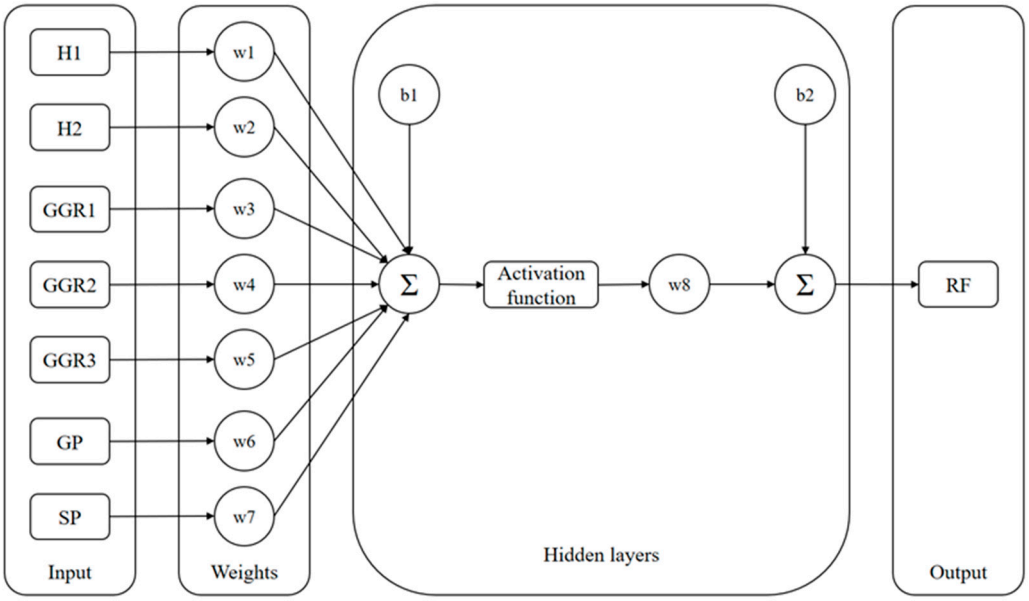

Figure 7. The Artificial Neural Network architecture comprises three layers (inputs, hidden, and outputs) and three mathematical equations (weights, activation, and summation functions).

Table 13. Weights for reduction factors' prediction related to dropping the backfill material.

Weights		36 Data Database	252 Data Database
w_H			
	H1	−0.50487	1.49953
	H2	−1.08017	−0.65195
w_{GGR}			
	GGR1	−0.75023	−2.92709
	GGR2	−0.57875	0.17595
	GGR3	−0.51103	1.38466
w_B			
	SP	−0.72347	1.94361
	GP	−1.23944	0.97083
Weights			
	b_1	0.68053	−0.42686
	b_2	0.36379	−0.36104
	w_8	−0.27650	−0.05205

The weights shown in Table 13 (some with negative values) give an awkward first impression of the *RF*'s prediction equation. As the lower reduction factor predicted is equal to 1.00, it can be expected that the summation function results in a negative value that provides a positive value when multiplied by the negative values of w_8. The final summation with b_2 results in a positive *RF* value. These occur because the weights were obtained based on a series of back and forward propagations in the Artificial Neural Networks that culminate in weight values for the most accurate prediction. Thus, the prediction equation combines mathematical equations such as the summation and activation functions. It provides a very accurate *RF* prediction, with relative errors equal to 3.57% for the smallest database (composed of 36 data) and a relative error equal to 7.52 for the broader database (252 data).

3.3.2. Multiple Linear Regression

Table 14 shows that the coefficients obtained for the drop height parameters were not significant (coefficients with a *p*-value > 0.1) in the second database (comprising 252 data). Additionally, the coefficient of determination (R^2) decreases with the increase in data in the databases. For a variable to be considered significant, the probability of obtaining a result as extreme or more extreme than the observed result, assuming that the null hypothesis is true, must be less than the *p*-value. Although the R^2 values were small and indicated low representativeness of the model, the *p*-values for the model are very close to zero, indicating that the regression model explains/represents the variation in the *RF* variable. Some variables show strong correlations due to the databases' dichotomous structure (for example, the drop heights H1 and H2 and the backfill materials GP and SP). This can be observed in Table 14, where the highly correlated coefficients presented are "NA."

Table 14. Estimated parameters and R^2 to predict the reduction factor for the ultimate tensile strength related to dropping the backfill material by Multiple Linear Regression (MLR).

Variables and Coefficients	36 Data Database	252 Data Database
R^2	0.6582	0.422
p-value	1.07×10^{-7}	2.2×10^{-22}
H1	−0.02278	−0.02382 *
H2	NA	NA
GGR1	0.19	0.19122
GGR2	0.035	0.035 *
GGR3	NA	NA
SP	−0.04167	−0.04324
GP	NA	NA

Note: * coefficients with a *p*-value > 0.1; NA: coefficients of variables in the model have a perfect linear relationship. Thus, only some regression coefficients in the model can be estimated.

According to the residues' analysis for the smaller database (36 data; Figure 8), there is a normal distribution and homoscedasticity. The databases' residues did not attend to the normality supposition required in the Shapiro–Wilk test. Moreover, the residues of both databases have shown homoscedasticity, a condition that does not satisfy the requirements for applying the Multiple Linear Regression (MLR) methods. Thus, adopting Artificial Neural Networks (ANNs) can be seen as an exciting alternative solution to obtain a prediction equation for the reduction factor since it does not have such mathematical constraints for its application.

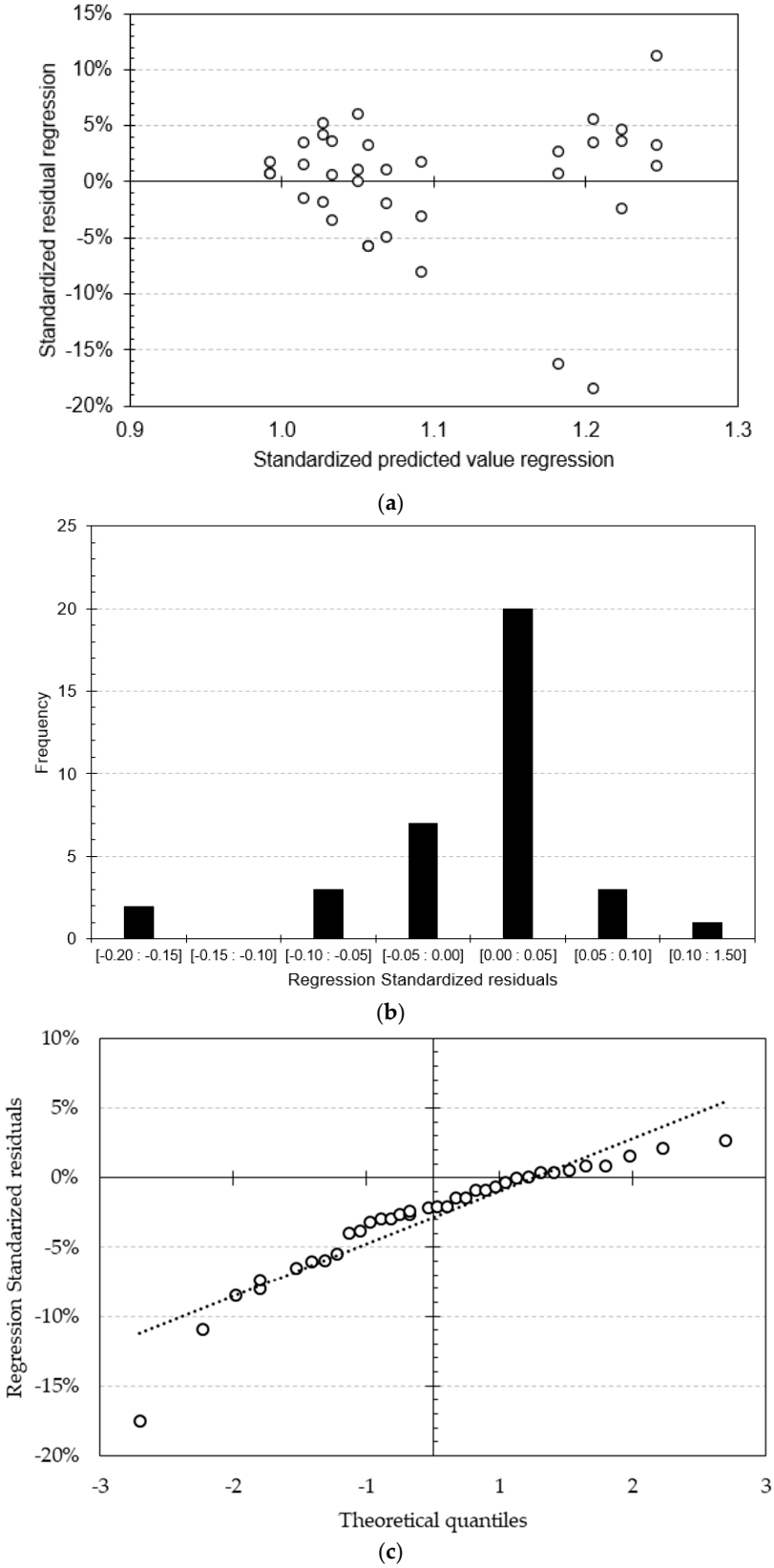

Figure 8. Residuals analysis for the dichotomous database composed of 36 data: (**a**) histogram; (**b**) Q-Q normal regression chart, and (**c**) scatter plot.

4. Conclusions

This present study aimed to investigate the damage caused by dropping backfilling materials on geogrids and propose a prediction equation for the reduction factors resulting from this damage. Six different backfills were dropped using a wheel loader from heights of 1.0 m and 2.0 m over geogrid meshes; the specimens were carefully exhumed and tested under tensile loading. The results were validated using a statistical tool, and then the reduction factors were calculated and composed databases submitted to machine learning to provide the prediction equations. Based on the study results, the following conclusions can be drawn:

- No strong relationship was observed between the backfills' grain-size distribution parameters and the reductions caused by the damage induced. Similarly, the potential energy could not be directly correlated with the damage induced, which indicates that the increase in the drop height cannot be associated with an increase in damage. However, it was noted that the damage affected the geogrids' tensile strength, strain at failure, and secant tensile stiffness differently.
- The geogrids' tensile strength is affected differently according to the backfill grain size distribution. Backfills with a more uniform gradation cause damage to increase as the maximum grain size of the backfill and the drop height increase. Conversely, the damage is primarily influenced by the backfill grain size distribution (curvature), whereas the maximum grain size is taken as a secondary aspect for backfills with continuous gradation. For these backfills, the tensile strength reduction was very similar regardless of the drop height and exhibited a slight increase as the maximum grain size of the backfill increased.
- The strain at failure was nearly unaffected by the damage induced. However, it was noted that a significant increase in its variability occurred. On the contrary, secant tensile stiffness is the most significantly affected property of interest and has shown a randomized behavior for each geogrid investigated. The results suggest that the damage induced by the drop height caused elastic deformation in the geogrids, compromising their secant tensile stiffness. However, further investigations are required to validate this assumption.
- Regarding the reduction factors, the PVA geogrid is the most sensitive to the induced damage because it is low-coated and exhibits lower bending stiffness than the PET geogrids. Considering the PET geogrids, the material with the lowest ultimate tensile strength was more affected in terms of tensile strength; meanwhile, the material with a higher ultimate tensile strength was more affected concerning the secant tensile stiffness. Moreover, a second method to calculate the reduction factors was proposed that proved to be slightly conservative (resulting in a reduction factor, on average, 2.3% higher than those from the traditional method adopted in the literature).
- The databases obtained from this experimental investigation do not meet the criteria for using multiple linear regression to predict the reduction factors. However, the artificial neural network is an interesting alternative that has accurately predicted the reduction factors with errors lower than 8% compared to those derived from the experimental investigation.

This study does not try to incorporate a new reduction factor to determine the geogrids' characteristic tensile strength (to be adopted in design). The results obtained herein highlighted that backfill drop material is responsible for causing damage to the geogrids. Further investigations are required to investigate the effect of the dropping process on different geosynthetic materials. Moreover, the study proposes that the data obtained by experimental tests can be used to predict design parameters using machine learning techniques. Finally, the study encourages the potential application of this technique (or similar ones) to evaluate the reduction factor's data already available in the literature to provide a more comprehensive prediction equation.

Author Contributions: The individual contributions of each author are highlighted as follows: Conceptualization, M.P.F. and J.L.d.S.; methodology, M.P.F.; software, G.K.K. and A.L.B.N.C.; validation, M.P.F., G.K.K. and F.B.F.; formal analysis, M.P.F. and G.K.K.; investigation, M.P.F.; resources, J.L.d.S.; data curation, M.P.F., G.K.K., C.S.P. and A.L.B.N.C.; writing—original draft preparation, M.P.F. and G.K.K.; writing—review and editing, J.L.d.S., C.S.P., A.L.B.N.C. and F.B.F.; supervision, J.L.d.S., C.S.P., and A.L.B.N.C.; project administration, J.L.d.S.; funding acquisition, J.L.d.S. All authors have read and agreed to the published version of the manuscript.

Funding: This research was funded by Coordenação de Aperfeiçoamento de Pessoal de Nível Superior (CAPES), grant number: 001. F.B.F. wishes to acknowledge Grant No. 2021.03625.CEECIND from the Stimulus of Scientific Employment, Individual Support (CEECIND)—4th Edition provided by Fundação para a Ciência e Tecnologia (FCT); and Base Funding—UIDB/04708/2020 of the CONSTRUCT—Instituto de I&D em Estruturas e Construções—funded by national funds through the FCT/MCTES (PIDDAC).

Institutional Review Board Statement: Not applicable.

Informed Consent Statement: Not applicable.

Data Availability Statement: Data will be made available on request.

Acknowledgments: The authors would like to thank the University of São Paulo, the National Council for Scientific and Technological Development (CNPq), São Paulo Research Foundation (FAPESP), RENOVE Waste Management, Huesker Geosynthetics, and Eletrobras FURNAS. This study was financed in part (with support granted to the first author) by the Brazilian Ministry of Education (Coordenação de Aperfeiçoamento de Pessoal de Nível; CAPES)—Finance Code 001.

Conflicts of Interest: The authors declare no conflict of interest.

References

1. Siqueira-Gay, J.; Sonter, L.J.; Sánchez, L.E. Exploring potential impacts of mining on forest loss and fragmentation within a biodiverse region of Brazil's northeastern Amazon. *Resour. Policy* **2020**, *67*, 101662. [CrossRef]
2. Escavy, J.I.; Herrero, M.J.; Lopez-Acevedo, F.; Trigos, L. The progressive distancing of aggregate quarries from the demand areas: Magnitude, causes, and impact on CO_2 emissions in Madrid Region (1995–2018). *Resour. Policy* **2022**, *75*, 102506. [CrossRef]
3. Akana, A.O.; Ikegbunam, F.I. Natural Resource Exploitation in Nigeria: Consequences of Human Actions and Best Practices for Environmental Sustainability—A Review. *Sparkling Int. J. Multidiscip. Res. Stud.* **2019**, *2*, 1–14.
4. Langer, W.H.; Abogast, B.F. Environmental Impacts of Mining Natural Aggregate. In *Deposit and Geoenvironmenal Models for Resource Exploitation and Environmental Security*; Fabbri, A.G., Gaál, G., McCammon, R.B., Eds.; Part 2: NATO Science Series; Springer: Dordrecht, The Netherlands, 1998; pp. 151–169.
5. Al-Awadhi, J.M. Impact of gravel quarrying on the desert environment of Kuwait. *Environ. Geol.* **2001**, *41*, 365–371. [CrossRef]
6. Arulrajah, A.; Piratheepan, J.; Bo, M.W.; Sivakugan, N. Geotechnical characteristics of recycled crushed brick blends for pavement sub-base applications. *Can. Geotech. J.* **2012**, *49*, 796–811. [CrossRef]
7. Melbouci, B. Compaction and shearing behaviour study of recycled aggregates. *Constr. Build. Mater.* **2009**, *23*, 2723–2730. [CrossRef]
8. Aqil, U.; Rarsuoka, F.; Uchimura, T.; Lohani, T.N.; Tomita, Y.; Matsushima, L. Strength and deformation characteristics of recycled concrete aggregate as backfill material. *Soils Found.* **2005**, *45*, 53–72. [CrossRef]
9. Esin, T.; Cosgun, N. A study conducted to reduce construction waste generation in Turkey. *Building* **2007**, *42*, 1667–1674. [CrossRef]
10. Kartam, N.; Al-mutairi, N.; Al-ghusain, I.; Al-humoud, J. Environmental management of construction and demolition waste in Kuwait. *Waste Manag.* **2004**, *24*, 1049–1059. [CrossRef]
11. Mckelvey, D.; Sivakumar, Ã.V.; Bell, A.; Mclaverty, G. Shear strength of recycled construction materials intended for use in vibro ground improvement. *Gr. Improv.* **2002**, *6*, 59–68. [CrossRef]
12. Touahamia, M.; Sivakumar, V.; McKelvey, D. Shear strength of reinforced-recycled material. *Constr. Build. Mater.* **2002**, *16*, 331–339. [CrossRef]
13. Arulrajah, A.; Piratheepan, J.; Aatheesan, T.; Bo, M.W. Geotechnical Properties of Recycled Crushed Brick in Pavement Applications. *J. Mater. Civ. Eng.* **2011**, *23*, 1444–1542. [CrossRef]
14. Cameron, D.A.; Azam, A.H.; Rahman, M.M. Recycled clay mansonry and recycled concrete aggregate blends in pavement. In Proceedings of the GeoCongress 2012, Oakland, CA, USA, 25–29 March 2012; pp. 1532–1541.
15. Rahman, M.A.; Imteaz, M.; Arulrajah, A.; Disfani, M.M. Suitability of recycled construction and demolition aggregates as alternative pipe backfilling materials. *J. Clean. Prod.* **2014**, *66*, 75–84. [CrossRef]
16. Medina, C.; Zhu, W.; Howind, T.; Frías, M.; Rojas, M.I.S. De Effect of the constituents (asphalt, clay materials, floating particles and fines) of construction and demolition waste on the properties of recycled concretes. *Constr. Build. Mater.* **2015**, *79*, 22–33. [CrossRef]
17. *NBR 15116*; Recycled Aggregate of Solid Residue of Building Constructions—Requirements and Methodologie. ABNT (Brazilian Association of Technical Standards): Rio de Janeiro, Brazil, 2004.

18. Cardoso, R.; Vasco, R.; De Brito, J.; Dhir, R. Use of recycled aggregates from construction and demolition waste in geotechnical applications: A literature review. *Waste Manag.* **2015**, *49*, 131–145. [CrossRef]
19. Silva, R.V.; De Brito, J.; Dhir, R.K. Properties and composition of recycled aggregates from construction and demolition waste suitable for concrete production. *Constr. Build. Mater.* **2014**, *65*, 201–217. [CrossRef]
20. Banias, G.; Achillas, C.; Vlachokostas, C.; Moussiopoulos, N.; Tarsenis, S. Assessing multiple criteria for the optimal location of a construction and demolition waste management facility. *Build. Environ.* **2010**, *45*, 2317–2326. [CrossRef]
21. Blengini, G.A.; Garbarino, E. Resources and waste management in Turin (Italy): The role of recycled aggregates in the sustainable supply mix. *J. Clean. Prod.* **2010**, *18*, 1021–1030. [CrossRef]
22. Coelho, A.; De Brito, J. Economic viability analysis of a construction and demolition waste recycling plant in Portugal—Part II: Economic sensitivity analysis. *J. Clean. Prod.* **2013**, *39*, 329–337. [CrossRef]
23. Coelho, A.; De Brito, J. Economic viability analysis of a construction and demolition waste recycling plant in Portugal—Part I: Location, materials, technology and economic analysis. *J. Clean. Prod.* **2013**, *39*, 338–352. [CrossRef]
24. Rodríguez, G.; Medina, C.; Alegre, F.J.; Asensio, E.; De Sánchez Rojas, M.I. Assessment of Construction and Demolition Waste plant management in Spain: In pursuit of sustainability and eco-efficiency. *J. Clean. Prod.* **2015**, *90*, 16–24. [CrossRef]
25. Asgari, A.; Ghorbanian, T.; Yousefi, N.; Dadashzadeh, D.; Khalili, F.; Bagheri, A.; Raei, M.; Mahvi, A.H. Quality and quantity of construction and demolition waste in Tehran. *J. Environ. Health Sci. Eng.* **2017**, *15*, 14. [CrossRef] [PubMed]
26. Delongui, L.; Matuella, M.; Núñez, W.P.; Fedrigo, W.; Silva Filho, L.C.P.d.; Ceratti, J.A.P. Construction and demolition waste parameters for rational pavement design. *Constr. Build. Mater.* **2018**, *168*, 105–112. [CrossRef]
27. Garg, N.; Thompson, M. Lincoln Avenue reclaimed asphalt pavement base project. *Transp. Res. Rec.* **1996**, *1547*, 89–95. [CrossRef]
28. Arulrajah, A.; Piratheepan, J.; Ali, M.M.Y.; Bo, M.W. Geotechnical properties of recycled concrete aggregate in pavement sub-base applications. *Geotech. Test. J.* **2012**, *35*, 743–751. [CrossRef]
29. Herrador, R.; Pérez, P.; Garach, L.; Ordóñez, J. Use of Recycled Construction and Demolition Waste Aggregate for Road Course Surfacing. *J. Transp. Eng.* **2012**, *138*, 182–190. [CrossRef]
30. Leite, F.D.C.; Motta, R.D.S.; Vasconcelos, K.L.; Bernucci, L. Laboratory evaluation of recycled construction and demolition waste for pavements. *Constr. Build. Mater.* **2011**, *25*, 2972–2979. [CrossRef]
31. Ossa, A.; García, J.L.; Botero, E. Use of recycled construction and demolition waste (CDW) aggregates: A sustainable alternative for the pavement construction industry. *J. Clean. Prod.* **2016**, *135*, 379–386. [CrossRef]
32. Albayati, A.; Wang, Y.; Wang, Y.; Haynes, J. A sustainable pavement concrete using warm mix asphalt and hydrated lime treated recycled concrete aggregates. *Sustain. Mater. Technol.* **2018**, *18*, e00081. [CrossRef]
33. Al-Mosawe, H.; Albayati, A.; Wang, Y.; Mashaan, N.S. An Experimental Study of Granular Material Using Recycled Concrete Waste for Pavement Roadbed Construction. *Buildings* **2022**, *12*, 1926. [CrossRef]
34. Bessa Ferreira, F.; Pereira, P.; Silva Vieira, C.; Lurdes Lopes, M. Long-Term Tensile Behavior of a High-Strength Geotextile after Exposure to Recycled Construction and Demolition Materials. *J. Mater. Civ. Eng.* **2022**, *34*, 04022046. [CrossRef]
35. Ferreira, F.B.; Vieira, C.S.; Mendonça, G.; Lopes, M.d.L. Effect of Sustained Loading on the Direct Shear Behaviour of Recycled C&D Material–Geosynthetic Interfaces. *Materials* **2023**, *16*, 1722. [CrossRef] [PubMed]
36. Santos, E.C.G.; Palmeira, E.M.; Bathurst, R.J. Behaviour of a geogrid reinforced wall built with recycled construction and demolition waste backfill on a collapsible foundation. *Geotext. Geomembr.* **2013**, *39*, 9–19. [CrossRef]
37. Santos, E.C.G.; Palmeira, E.M.; Bathurst, R.J. Construction of a full-scale wrapped face geogrid reinforced wall using recycled construction and demolition waste as backfill material. In Proceedings of the 9th International Conference on Geosynthetics—Geosynthetics: Advanced Solutions for a Challenging World, ICG 2010, São Paulo, Brazil, 23 May 2010; pp. 1769–1772.
38. Rathje, E.M.; Rauch, A.F.; Trejo, D.; Folliard, K.J.; Viyanant, C.; Esfellar, M.; Jain, A.; Ogalla, M. *Evaluation of Crushed Concrete and Recycled Asphalt Pavement as Backfill for Mechanically Stabilized Earth Walls*; Center for Transportation Research (CTR): Austin, TX, USA, 2006.
39. Santos, E.C.G.; Palmeira, E.M.; Bathurst, R.J. Performance of two geosynthetic reinforced walls with recycled construction waste backfill and constructed on collapsible ground. *Geosynth. Int.* **2014**, *21*, 256–269. [CrossRef]
40. Vieira, C.S.; Pereira, P.M. Interface shear properties of geosynthetics and construction and demolition waste from large-scale direct shear tests. *Geosynth. Int.* **2016**, *23*, 62–70. [CrossRef]
41. Vieira, C.S. Valorization of Fine-Grain Construction and Demolition (C&D) Waste in Geosynthetic Reinforced Structures. *Waste Biomass Valorization* **2018**, *12*, 1615–1626. [CrossRef]
42. Soleimanbeigi, A.; Tanyu, B.F.; Aydilek, A.H.; Florio, P.; Abbaspour, A.; Dayioglu, A.Y.; Likos, W.J. Evaluation of recycled concrete aggregate backfill for geosynthetic-reinforced MSE walls. *Geosynth. Int.* **2019**, *26*, 396–412. [CrossRef]
43. Allen, T.M.; Bathurst, R.J. Combined Allowable Strength Reduction Factor for Geosynthetic Creep and Installation Damage. *Geosynth. Int.* **1996**, *3*, 407–439. [CrossRef]
44. FHWA (Federal High Way Administration). *Design and Construction of Mechanically Stabilized Earth Walls and Reinforced Soil Slopes*; Berg, R.R.I., Christopher, B.R., Samtani, N.C., Eds.; FHWA: Washington, DC, USA, 2010; Volume I, ISBN FHWA-NHI-10-024.
45. Rosete, A.; Lopes, P.M.; Pinho-Lopes, M.; Lopes, M.L. Tensile and hydraulic properties of geosynthetics after mechanical damage and abrasion laboratory tests. *Geosynth. Int.* **2013**, *20*, 358–374. [CrossRef]
46. Hufenus, R.; Rüegger, R.; Flum, D.; Sterba, I.J. Strength reduction factors due to installation damage of reinforcing geosynthetics. *Geotext. Geomembr.* **2005**, *23*, 401–424. [CrossRef]

47. Fleury, M.P.; Santos, E.C.G.; Lins da Silva, J.; Palmeira, E.M. Geogrid installation damage caused by recycled construction and demolition waste. *Geosynth. Int.* **2019**, *26*, 641–656. [CrossRef]
48. Cazzuffi, D.; Mongiovi, L.; Torresendi, M. Laboratory and field tests for the evaluation of installation damage of geosynthetics in reinforced earth structures. In Proceedings of the 15th International Conference on Soil Mechanics and Geotechnical Engineering, Instanbul, Turkey, 27–31 August 2001; pp. 1565–1568.
49. Austin, R.A. The effect of installation activities and fire exposure on geogrid performance. *Geotext. Geomembr.* **1997**, *15*, 367–376. [CrossRef]
50. Richardson, G.N. Field evaluation of geosynthetic survivability in aggregate road base. *Geotech. Fabr. Rep.* **1998**, *16*, 34–38.
51. Hsieh, C.W.; Wu, J.H. Installation survivability of flexible geogrids in various pavement subgrade materials. *Transp. Res. Rec.* **2001**, *1772*, 190–196. [CrossRef]
52. Lim, S.Y.; McCartney, J.S. Evaluation of effect of backfill particle size on installation damage reduction factors for geogrids. *Geosynth. Int.* **2013**, *20*, 62–72. [CrossRef]
53. Pinho-lopes, M.; Lopes, M.L. Tensile properties of geosynthetics after installation damage. *Environ. Geotech.* **2014**, *1*, 161–178. [CrossRef]
54. Santos, E.C.G.; Bueno, B.S.; Palmeira, E.M. Strength reduction of geosynthetics used in RSW built with RCDW as backfill material. In Proceedings of the 5th European Conference on GEosynthetics-EuroGeo 5, Valencia, Spain, 19 September 2012; pp. 481–485.
55. Vieira, C.S.; Pereira, P.M. Damage induced by recycled Construction and Demolition Wastes on the short-term tensile behaviour of two geosynthetics. *Transp. Geotech.* **2015**, *4*, 64–75. [CrossRef]
56. Vieira, C.S.; Lopes, M.D.L. Damage Induced by Recycled Aggregates on the Short-Term Tensile Behaviour of a High-Strength Geotextile. *Procedia Eng.* **2016**, *143*, 212–219. [CrossRef]
57. Domiciano, M.L.; Santos, E.C.G.; Lins da Silva, J. Geogrid Mechanical Damage Caused by Recycled Construction and Demolition Waste (RCDW): Influence of Grain Size Distribution. *Soils Rocks* **2020**, *43*, 231–246. [CrossRef]
58. Barbosa, F.A.S.; Santos, E.C.G. Geogrid mechanical damages due to recycled construction and demolition wastes. In Proceedings of the 14th International Waste Management and Landfill Symposium, Sardegna, Italy, 30 September 2013.
59. Abuel-naga, H.M.; Bouazza, A. Geotextiles and Geomembranes Numerical experiment-arti fi cial intelligence approach to develop empirical equations for predicting leakage rates through GM/GCL composite liners. *Geotext. Geomembr.* **2014**, *42*, 236–245. [CrossRef]
60. Ismail, A.; Jeng, D. Engineering Applications of Artificial Intelligence Modelling load—Settlement behaviour of piles using high-order neural network (HON-PILE model). *Eng. Appl. Artif. Intell.* **2011**, *24*, 813–821. [CrossRef]
61. Moayedi, H.; Gör, M.; Khari, M.; Kok, L.; Bahiraei, M.; Tien, D. Hybridizing four wise neural-metaheuristic paradigms in predicting soil shear strength. *Measurement* **2020**, *156*, 107576. [CrossRef]
62. Raja, M.N.A.; Shukla, S.K. Predicting the settlement of geosynthetic-reinforced soil foundations using evolutionary artificial intelligence technique. *Geotext. Geomembr.* **2021**, *49*, 1280–1293. [CrossRef]
63. Fleury, M.P.; Kamakura, G.K.; Pitombo, C.S.; Cunha, B.N.; Lins, J. *Geotextiles and Geomembranes Prediction of Non-Woven Geotextiles' Reduction Factors for Damage Caused by the Drop of Backfill Materials*; Elsevier: Amsterdam, The Netherlands, 2023. [CrossRef]
64. Petrik, P.M.; Baslík, R. Design of geotextiles reinforcing embankments with reference to long-term loading. *Geotext. Geomembr.* **1988**, *7*, 71–79. [CrossRef]
65. *NBR NM 248*; Aggregates—Sieve Analysis of Fine and Coarse Aggregates. ABNT (Brazilian Association of Technical Standards): Rio de Janeiro, Brazil, 2003.
66. *NBR 7809*; Coarse Aggregate—Determination of shape index by the caliper—Method of test ICS. ABNT (Brazilian Association of Technical Standards): Rio de Janeiro, Brazil, 2019.
67. *ASTM D 2487-00*; Standard Practice for Classification of Soils for Engineering Purposes (Unified Soil Classification System). ASTM (American Society for Testing and Materials): West Conshohocken, PA, USA, 2006.
68. Barbosa, F.A.S.; Silva, E.M.; Santos, E.C.G. Polypropylene (PP) geosynthetics strength reduction due installation damages caused by construction and demolition waste (RCDW) [in Portuguese]. In Proceedings of the 16th Brazilian Conference of Soils Mechanics and Geotechnical Engineering-COBRAMSEG 2016, Belo Horizonte, Brazil, 19–22 October 2016.
69. Allen, T.M.; Bathurst, R.J. Characterization of Geostynthetic Load-Strain Behavior After Installation Damage. *Geosynth. Int.* **1994**, *1*, 181–199. [CrossRef]
70. *ASTM D 6637-15*; Standard Test Method for Determining Tensile Properties of Geogrids by the Single or Multi-Rib Tensile Method. ASTM (American Society for Testing and Materials): West Conshohocken, PA, USA, 2015. [CrossRef]
71. Paula, A.M.; Pinho-Lopes, M.; Lopes, M.L. Damage during installation laboratory test: Influence of the type of granular material. In Proceedings of the Third European Geosynthetics Conference, Munich, Germany, 1–3 March 2004; p. 4.
72. Huang, C.-C.; Liao, C.C. Abrasion damage of geogrids induced by turbid flow. *Geotext. Geomembr.* **2007**, *25*, 128–138. [CrossRef]
73. Pinho-Lopes, M.; Paula, A.M.; Lopes, M.L. Long-term response and design of two geosynthetics: Effect of field installation damage. *Geosynth. Int.* **2018**, *25*, 98–117. [CrossRef]
74. Raschka, S.; Mirjalili, V. *Python Machine Learning*, 3rd ed.; Malysiak, J., Ed.; Packt Publishing Ltd.: Birmingham, UK, 2019; ISBN 9781789955750.
75. Huang, C.-C. Laboratory simulation of installation damage of a geogrid. *Geosynth. Int.* **2006**, *13*, 120–132. [CrossRef]

76. Huang, C.C.; Chiou, S.L. Investigation of installation damage of some geogrids using laboratory tests. *Geosynth. Int.* **2006**, *13*, 23–35. [CrossRef]
77. Cho, S.D.; Lee, K.W.; Cazzuffi, D.A.; Jeon, H.Y. Evaluation of combination effects of installation damage and creep behavior on long-term design strength of geogrids. *Polym. Test.* **2006**, *25*, 819–828. [CrossRef]
78. Paula, A.M.; Pinho-Lopes, M.; Lopes, M.L. Effect of damage during installation on the mechanical behaviour of a biaxial woven polyester geogrid. In Proceedings of the 5th European Geosynthetic Congress-EUROGEO 5, Valencia, Spain, 16–19 September 2012; pp. 446–451.